applied sciences

MDPI

Article

Nanocomposites Photocatalysis Application for the Purification of Phenols and Real Olive Mill Wastewater through a Sequential Process

Srikanth Vuppala [1,*] and Marco Stoller [2]

[1] Department of Civil and Environmental Engineering, Politecnico di Milano, Piazza Leonardo da Vinci 32, 20133 Milan, Italy
[2] Department of Chemical Materials Environmental Engineering, University of Rome "La Sapienza", Via Eudossiana 18, 00184 Rome, Italy; marco.stoller@uniroma1.it
* Correspondence: nagavenkata.vuppala@polimi.it

Received: 14 September 2020; Accepted: 16 October 2020; Published: 20 October 2020

Abstract: In this study, a synthetic phenol solution of water and raw olive mill wastewater (OMW) were considered to achieve purification of the aqueous streams from pollutants. Only OMW was initially submitted to a coagulation/flocculation process, to reduce the turbidity, phenols, and chemical oxygen demand (COD). This first treatment appeared to be mandatory in order to remove solids from wastewater, allowing the successive use of laboratory-made core-shell nanocomposites. In detail, the optimal coagulant concentration, i.e., chitosan, was 500 mg/L, allowing a reduction of the turbidity and the COD value by 90% and 33%, respectively. After this, phenol wastewater was tested for photocatalysis and then OMW was treated by employing the laboratory-made nanocomposites in a photoreactor equipped with visible light sources and using optimal catalyst concentrations, which allowed for an additional 45% reduction of the COD of the OMW. In addition to this, the effect of the operating temperature was investigated on the photocatalytic process, and suitable kinetic models proposed.

Keywords: advanced oxidation processes; COD; N-TiO_2/FM; OMW; phenols; SDR

1. Introduction

Nanotechnology is considered to be a "key technology" in the future and its contribution to water and wastewater treatment innovations has already been significantly high. The word nanotechnology includes a wide range of technologies performed on a nanometer scale for many applications [1]. Nanomaterials have been widely used for various environmental applications, such as the treatment of complex wastewaters, showing significant removal efficiency for both organic and inorganic contaminants [2,3].

Mediterranean countries are major producers of olive oil, and as a consequence, olive mill wastewater (OMW). The composition of OMW may vary much and depends on the type of processed olives, their ripeness, and the extraction process adopted (traditional press method or centrifugation method) [4]. The treatment of OMW is a challenging task due to the high pollutant load (in terms of chemical oxygen demand (COD)), high concentration of recalcitrant compounds (namely lignins and tannins), long-chain fatty acids, phenolic compounds, and biotoxicity [5]. Therefore, for its treatment and disposal, OMW requires a feasible solution from a technical and economical point of view [6]. Recently, a vast number of studies have been reported on the development of chemical and biological technologies for the degradation of organic and inorganic pollutants in aqueous matrices [7]. Efficient and novel methods such as advanced oxidation processes (AOPs) have been considered as one

of the best technologies for treating a wide range of recalcitrant materials such as organic pollutants from water and wastewater [8]. Application of solar TiO_2 photocatalysis and solar photo-Fenton for OMW processing was reported initially, with 85% COD and up to 100% of phenol index removal in OMW [9]. Sustainable technologies for agro-food industry wastewater treatment to valorization is another potential aspect, which would reduce global climate change [10,11]. The phenolic compounds extraction from OMW and their benefits are reported by several studies [12,13].

Physical–chemical processes such as coagulation–flocculation and oxidation have also been employed in OMW treatment since both are simple and cheap, as well as easy to operate. Additional chemicals are used in these processes to destabilize the suspended and colloidal matter of OMW to form an insoluble solid that can be removed easily from the waste. Oil, suspended solids, COD, and biological oxygen demand (BOD) are decreased in this way. Destabilization of these colloids can be achieved either by reducing or increasing pH (neutralization) or by the addition of coagulants [14]. Chitosan is the only natural animal-based organic coagulant successfully tested. Chitosan itself is a nontoxic biopolymer and has a wide variety of applications in the fields of biotechnology, biomedical, environmental, microbiology, and pharmaceutical studies [15].

Phenols species, which may also be indicated as total phenols or phenolics, are widely employed in many manufacturing processes [16,17]. Phenol is highly toxic and carcinogenic compound and more resistant to degradation by many biological treatments or chemical adsorption processes. However, it may cause serious damage to human and animal ecosystems because of its inertness, toxicity, endocrine-disrupting abilities, and carcinogenic behavior. Phenols can be removed by physical processes such as flocculation, precipitation, adsorption onto granular activated carbon (GAC), or reverse osmosis (RO) [18].

Commonly used approaches are often ineffective because they simply haul the organic pollutants from water to another medium without degrading or mineralizing them. Among AOPs, the Fenton-like process is considered as a widely investigated method for wastewater treatment [19,20]; recently, the photo-Fenton process was applied to OMW treatment and achieved 80% microcontaminant degradation [21]. In recent years, to remove or mineralize the organic pollutants, the sorption [22,23] and heterogeneous photocatalysis methods have been widely adopted, deriving from modern advanced oxidation processes (AOPs) [24–26].

Recent overwhelming research interest in using titanium dioxide (TiO_2) as a photocatalyst is attributed to the excellent capabilities of this catalyst to degrade a wide array of organic compounds in CO_2 and H_2O. Several studies reported TiO_2 used in suspension form in wastewater treatment, resulting in the slurry formation in photoreactors due to its fine powdery nature; this is one major limitation in TiO_2 based photocatalysis [27] and its moderate bandgap of 2.7 eV makes the catalyst active only in the UV region [28]. The photochemical side reactions and decomposition of catalyst causes the fast termination of photocatalytic cycles and limit the efficiency of the process, and also leads to fastback electron transfer processes and recombination reactions that are the reasons for limiting the photocatalysis performance [29]. Much attention has been paid by several research groups on the modification of TiO_2 surface area, mainly by the atomic mixing with SiO_2 to enhance the activity of TiO_2 catalyst [30]. Nevertheless, as SiO_2 is inserted in the TiO_2 lattice, the improvement of the specific surface area of the resulting catalyst is also accompanied by the broadening of its bandgap energy. Consequently, TiO_2-SiO_2 mixed oxide inherently absorbs much more UV light than the visible counterpart, compared to bare TiO_2. Although nitrogen-doped TiO_2 (N-TiO_2) catalyst has been intensively studied for the absorption of visible light, nitrogen-doped TiO_2-SiO_2 (N-TiO_2-SiO_2) catalyst has not been much explored. In this present research, the N-TiO_2-SiO_2 mixed oxide is synthesized using the sol-gel method. For simultaneous improvement of the specific surface area and crystallinity of N-TiO_2-SiO_2 catalyst, hydrothermal treatment is also employed immediately after the sol-gel process [31].

Many techniques are used for the deposition of TiO_2 onto silica-coated iron oxide nanoparticles (NPs). Impregnation, precipitation, and sol-gel methods are used. Magnetic visible–active

photocatalysts are promising materials for overcoming the two fundamental drawbacks of titanium dioxide: NPs that hinder TiO_2 application and development in the fields of environmental pollutants and energy sources. Recently, many techniques have been proposed to induce visible light activity and magnetic separability to TiO_2 NPs [32]. Very recently, large-scale synthesis of discrete and uniformly sized Fe-based nanoparticles and superparamagnetic Fe_3O_4/SiO_2, based on the use of spinning disk reactor (SDR), has been reported [15]. Fe-based metallic glass technique was reported for remediation of industrially contaminated water with arsenic and nitrate by mass production [33].

Among all the mixing devices used for precipitation, SDR has many advantages when compared to other mixing devices, such as the rotational speed grater. Good results on controlling size and shape of the nanoparticles and NPs production of narrow particle distribution size (PDSs) at a specific target size and also through continuous operation, compatible to industrial practice, can be performed [34]. The proposed work is also economically effective; the catalyst is reusable and reduces operating cost. This approach has been considered in order to achieve economic feasibility of the process since immobilized systems may not be used due to the high capacity of the wastewater. However, in this process suspended photocatalytic particles allow for the operation of the system without any interruption, and the catalyst could be reused for several cycles [32,35]. Nanoparticles can be produced for industrial purposes; the scale-up has been discussed in the previous work of one of the authors [15].

Therefore, the present work reports the pretreatment of real olive mill wastewater through the coagulation–flocculation process and subsequent photocatalytic degradation by employing laboratory synthesized Ti-based nanocatalysts. The photocatalytic method showed efficient removal of targeted pollutants (COD and phenols). A comparison with synthetic phenol solution degradation is reported, as well as the kinetic data interpretation through suitable mathematical modeling.

2. Materials and Methods

2.1. Materials

OMW samples were collected in the South of Lazio (Italy) from the local olive oil industry. In particular, the wastewater exits an oil extraction process based on the two-phase centrifugal method. The synthetic phenol solution procured was prepared at an initial concentration of 25 mg/L from phenol liquified 85% RE- Pure which was procured from Carlo Erba reagents. Five hundred mg of chitosan (from Sigma Aldrich-448877, with medium molecular weight and a degree of deacetylation at 75–85%) dissolved in 2.5 mL of 2 M HCl (from Sigma Aldrich 37%, ACS reagent grade) solution and 47.5 mL of deionized water. After 60 min, 50 mL of deionized water was added under mechanical stirring to produce 5 g/L chitosan stock solution [24]. The nanophotocatalyst was prepared according to a previous study where its characterization is also reported [32]. In brief, the nanoparticles are made of a magnetic core of Fe_3O_4, the first shell of SiO_2, and the second shell of TiO_2 N-doped.

All the reagents were purchased from Sigma Aldrich (Milan, Italy) and Carlo Erba (Milan, Italy) and all the solutions were prepared with deionized water.

2.2. Experimental

The OMW was initially sieved at 0.3 mm to remove the coarse particles. Subsequently, six 600 mL aliquots were added in 1000 mL volume tanks for the coagulation/flocculation process, performed through a Jar test apparatus. The coagulant (chitosan) concentration was varied in the range 100–800 mg/L, the coagulation time was 120 min at fixed pH (4.6, that of raw OMW). The turbidity of the OMW was measured at of 5 min time steps. The sedimentation step (24 h) followed the coagulation process and the generated sludge was removed before starting with the following photodegradation step.

The photocatalysis of OMW was performed in a photoreactor with a 400 mL volume (OMW volume used was 300 mL). The equipment setup and procedure is reported elsewhere in detail [32,36]. According to equal time steps of 15 min, an aliquot of OMW solution was withdrawn and the COD

was determined photometrically according to the Standard Methods for the Examination of Water and Wastewater, by standard procedure using a WTW CR4200 thermoreactor. Phenol concentrations were measured with a Merck Spectroquant® Pharo 100 spectrophotometer. The kinetic experiments were conducted at four different temperature (25 °C, 35 °C, 40 °C, and 45 °C) for pretreated OMW and synthetic phenol solution of 25 mg/L initial concentration. The optimal catalyst concentration was assessed based solely on the sorption results in the dark phase, varying the catalyst concentration in the range 1–3 g/L, which is the typical investigated range [37].

The turbidity was measured using an HF Scientific™ Micro 100 turbidimeter and the pH with a Crison pH-meter. The COD was measured according to the closed reflux colorimetric method [38] and the phenol concentration was measured by a UV-Vis spectrophotometer at 270 nm by observing the change in the absorbance at the maximum absorption wavelength (T80+, PG Instruments, Ltd., Wibtoft, UK). The concentration was then calculated from a calibration curve. The OMW was characterized by an initial COD value of 12.24 g/L and initial turbidity of 3.89 g/L. The pH of zero-charge of the catalyst was measured as equal to 6.55, through the method reported elsewhere [39], which was very close to the values reported in other studies [40,41]. All the experiments were conducted in duplicate and the average values are reported ($\sigma < 4\%$).

2.3. Mathematical Modeling

The kinetic data of turbidity variation over time of the OMW coagulation–flocculation process were interpreted according to Smoluchowski's theory (perikinetic model [42]):

$$\frac{dTur}{dt} = -\frac{4Tk_b\alpha_P Tur^2}{3\mu} \quad (1)$$

where k_b (J K^{-1}) is the Boltzmann constant, T (K) is the liquid volume temperature, Tur is the solid concentration (mg L^{-1}), α_P is the perikinetic probability factor, and ν (Pas) is the liquid dynamic viscosity. The following kinetic constant can be introduced:

$$k = \frac{4Tk_b\alpha_P}{3\mu} \quad (2)$$

Equation (1) can be analytically solved using the initial condition $Tur = Tur_0$ for $t = 0$, where $C0$ (mg L^{-1}) is the initial turbidity of the wastewater:

$$Tur = \frac{Tur_0}{1 + Tur_0 kt} \quad (3)$$

From the value of k (L mg^{-1} min^{-1}), Ani and coworkers [43] estimated the friction factor β to be equal to $\beta = 2r$, where r (kg min^{-1}) is the coagulation process rate. In addition, the Brownian diffusion coefficient D (m^2 min^{-1}), due to the existing concentration gradient driving force, can be estimated as:

$$D = \frac{k_b T}{\beta} \quad (4)$$

Since r decreases during the process, D undergoes an increase, up to reach the asymptotic r value. Regarding the photocatalytic kinetics interpretation, a pseudo-nth order kinetic model was used in a nonlinear regression of experimental data obtained at different operative temperature, based on COD removal for OMW treatment and phenol removal for synthetic phenol solution treatment:

$$C^{n_c-1} = \frac{C_0^{n_c-1}}{1 + (n_c - 1)C_0^{n_c-1}k_C t} \quad (5)$$

where C (mg/L) represents the COD or phenol concentration, the c-index of reaction order n, and kinetic constant k_C (L^{1+n}/min mg^{n-1}) indicates the COD case, which will be substituted by the p-index for the phenol case. The regressed kinetic constant values obtained at different initial temperatures were fitted to the Arrhenius model, expressed by the following equation:

$$k_C = k_0 \exp\left(-\frac{E}{RT}\right) \quad (6)$$

where R is the gas constant, E (J mol^{-1}) is the activation energy, k_0 (L^{1+n}/min mg^{n-1}) is the pre-exponential constant, and T (K) is the temperature. The nonlinear regression of experimental data was accomplished in the Excel environment, using the nonlinear solver of Excel (Microsoft).

3. Results and Discussion

3.1. Coagulation/Flocculation Results and Modeling

Figure 1 displays the OMW turbidity and COD values obtained at 120 min using different chitosan concentrations.

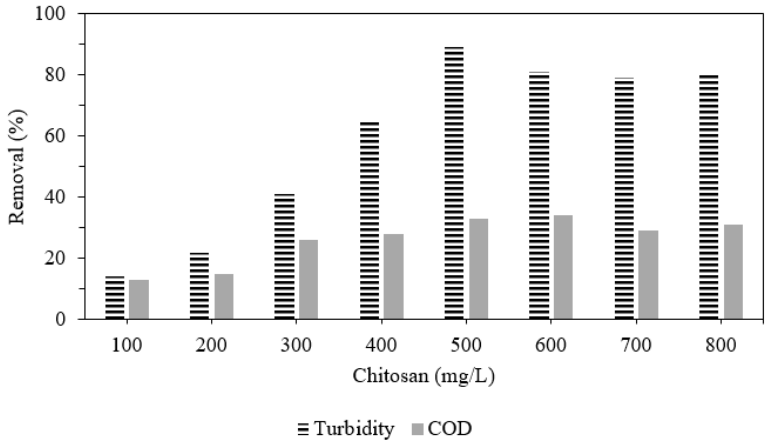

(**a**)

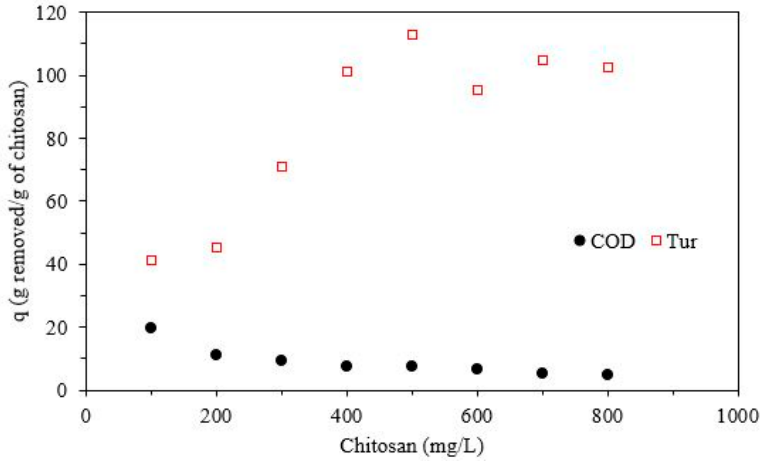

(**b**)

Figure 1. Coagulation/flocculation optimization tests results in terms of percentage removal (**a**) and of chemical oxygen demand/turbidity (COD/Tur) g removed/g of chitosan used (**b**) (temperature = 25 °C, initial pH = 4.6, initial COD = 12.24 g L^{-1}, initial turbidity = 3.89 g L^{-1}).

As reported in Figure 1a, the optimal chitosan concentration appears to be equal to 500 mg/L, very close to the optimal value found by other authors that treated similar OMW streams [44,45]. If one considers instead the optimal use of chitosan, it can be observed from Figure 1b that for COD removal, a better chitosan concentration would have been 100 mg/L, since a q_{COD} of 19.58 g/g was obtained, whereas for Tur removal, the optimal chitosan amount resulted to be again 500 mg/L (q_{Tur} = 112.93 g/g). The coagulation/flocculation step is fundamental for the subsequent AOPs technology applications in order to reduce the turbidity of the effluent. This aspect is important for the photocatalysis process, allowing the light to penetrate into the liquid volume with higher intensities. Another important result was the observed pH increase, that reached 5.6. Therefore, the first pretreatment allowed for the reduction of 90% of the initial turbidity and 33% of the initial COD, providing also a partial pH neutralization of the OMW. The COD reduction was mainly given by the sorption of organic acids and other surface-charged contaminants onto precipitated flocks, removed in the subsequent sedimentation process (sedimentation time equal to 24 h). As already observed in previous studies, a chitosan concentration above the optimum value increases the turbidity of the stream due to the restabilization mechanism typical to these processes. The results achieved can be compared with those reported in the literature for classical coagulants, such as the one reported by Nieto and coworkers [37] who observed a turbidity removal of about 90% on a real OMW using a commercial Nalco-77171.

Once the optimal coagulant concentration was fixed, the subsequent kinetic experiments were performed. Figure 2 reports the kinetic data results and modeling.

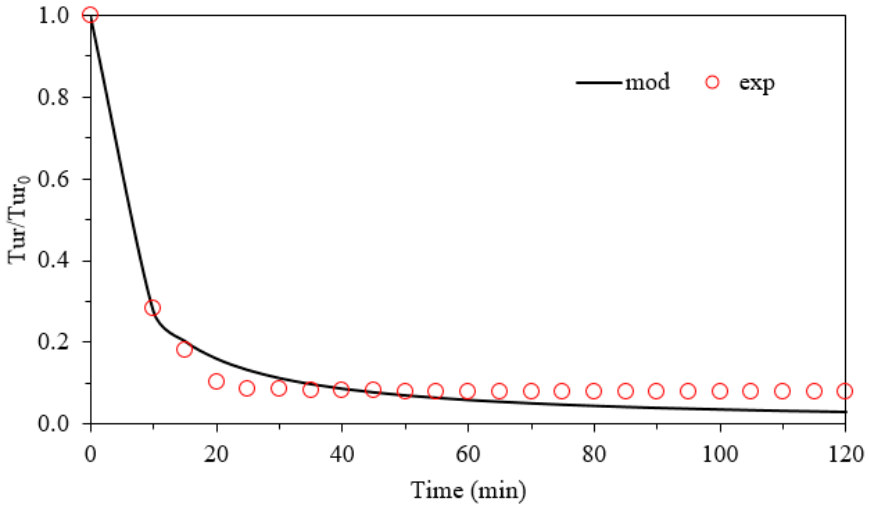

Figure 2. Olive mill wastewater (OMW) coagulation/flocculation kinetic results and modeling (chitosan concentration = 500 mg L^{-1}, temperature = 25 °C, initial turbidity 3.89 g L^{-1}).

The model was able to fit the overall experimental data well, including the asymptotic trend reached after 35–40 min. The second order of reaction was found to be suitable for this kind of mechanism, as demonstrated also by the high correlation coefficient, R2, obtained (0.98). The regressed kinetic constant was equal to 6.68 × 10^{-4} L/mg min, which result is close to the regressed value obtained by Kumar and coauthors, who modeled the coagulation kinetic of tannery wastewater by a pseudo-nth order kinetic model, obtaining a reaction order of 1.96 and a kinetic constant of 8.62 × 10^{-4} L/mg min [46]. From the kinetic constant value and rate values, the Brownian diffusion coefficient trend was estimated (Figure 3).

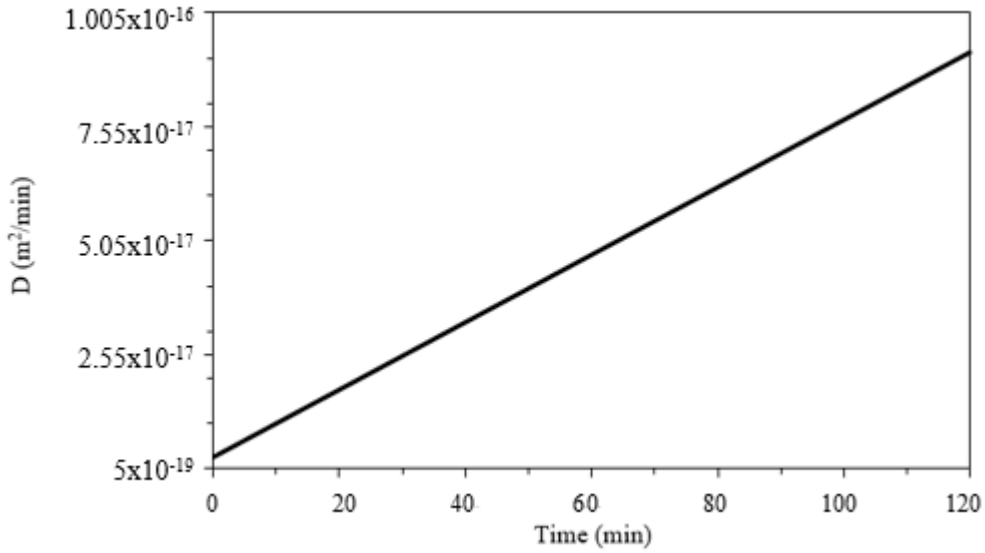

Figure 3. Diffusion coefficient (D) calculated trend (T = 25 °C, impeller rotational velocity = 20 rpm, time = 120 min, $\sigma < 4\%$).

The initial D value was 2.85×10^{-18} m^2/min and reached the maximum value of about 9.2×10^{-17} m^2/min at the end of the process. The reported values were characterized by the same order of magnitude as the D coefficients values calculated by Okolo and coworkers [47].

3.2. Photocatalysis Results and Modeling

Figure 4 reports the results of the catalyst concentration optimization step on both OMW and synthetic phenol solution.

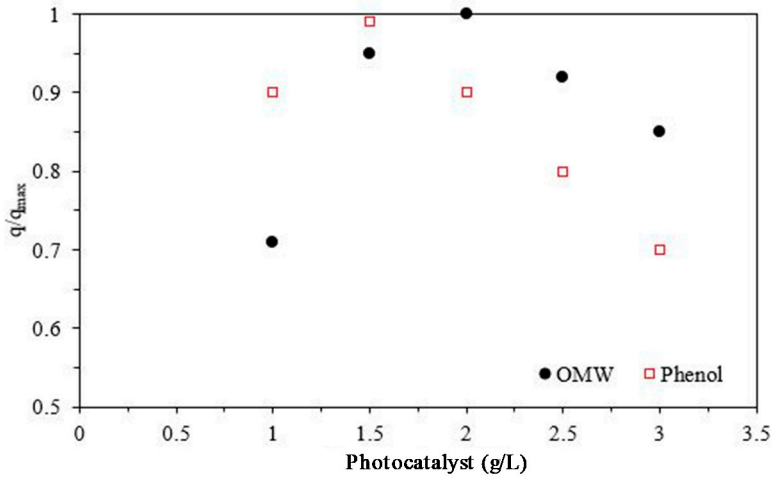

Figure 4. COD and phenols sorption removal obtained at a different photocatalyst concentration (T = 25 °C, initial OMW COD = 9.4 g L^{-1}, synthetic solution initial concentration = 25 mg L^{-1}, the contact time in dark = 30 min, q = mg of COD or phenols sorbed/g of photocatalyst and q_{max} is the maximum value of q, impeller rotational velocity = 200 rpm).

It is possible to observe that the optimal photocatalyst concentration was equal to 2 g L^{-1} (a similar value was obtained in previous work using the same catalyst but without N-doping [48]) and 1.5 g L^{-1} for OMW and synthetic phenol solution, respectively. The same experiments were conducted at T = 45 °C, the maximum value chosen for the experimental campaign, and it was observed that the optimal concentration values were the same as those used at lower temperature values, whereas the

q values underwent a slight reduction (about 7% for OMW and 10% for phenols). Another important result was that the pH of the pretreated OMW, 5.6, was lower in comparison to the pH of zero-charge of the photocatalyst, which resulted as positively charged and able to adsorb deprotonated organic acids and other negatively charged organic species present in the OMW.

Figure 5 reports the kinetic experimental and modeled data of OMW and synthetic phenol solution photodegradation.

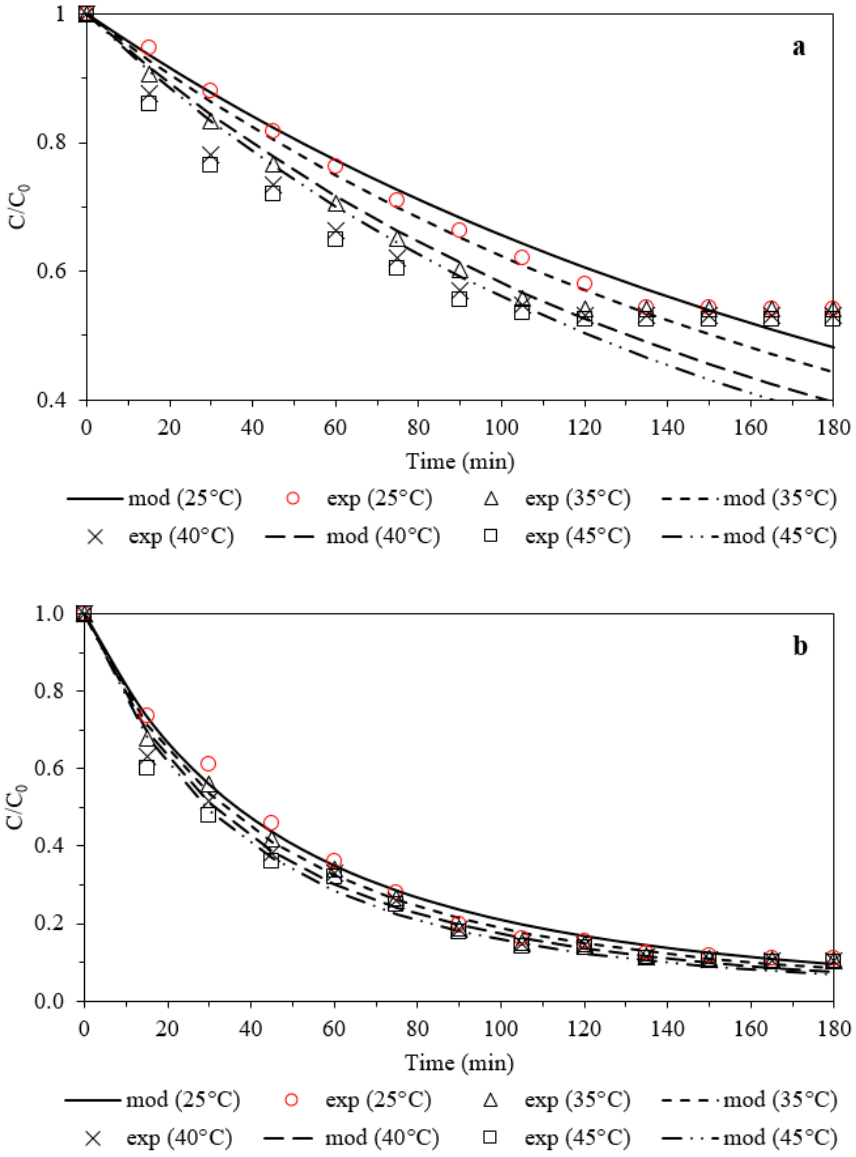

Figure 5. OMW (**a**) and synthetic phenol solution (**b**) kinetic photodegradation results and modeling at different T values (T = 25, 35, 40, and 45 °C; initial OMW COD = 9.4 g L^{-1}; synthetic solution initial concentration = 25 mg L^{-1}; impeller rotational velocity = 200 rpm).

In both cases, a T increase led to faster kinetics of the photodegradation process. In detail, the OMW COD removal efficiency at 180 min was equal to 45.8, 46.1, 47, and 47.3% for T = 25, 35, 40, and 45 °C, respectively, showing that the temperature increase did not modify substantially the asymptotic value, whereas it influenced the apparent kinetic constant k_C, which increased from 4.94×10^{-4} L^{1+n}/min mg^{n-1} at 25 °C to 6.91×10^{-4} L^{1+n}/min mg^{n-1} at 45 °C, with a reaction order always in the range 1.24–1.25. The COD removal efficiency was higher than that reported in a previous study where the same catalyst without N-doping was used in similar operative conditions [48]. In a

recent study of OMW, the photo-Fenton treatment at neutral pH was active only for a few minutes due to stability issues, and 80% microcontaminants degradation was reported. However, the photo-Fenton efficiency was tested in diluted OMW, and it would be not possible to reuse the catalyst [21]. In this study, the catalyst could be reused and there were no stability issues observed.

Regarding the results of synthetic phenol solution photodegradation, the phenols removal efficiency at 180 min was equal to 89.4, 89.9, 90.1, and 90.5% for T = 25, 35, 40, and 45 °C, respectively, whereas the apparent kinetic constant k_P values were 5.8×10^{-3}, 6.3×10^{-3}, 6.5×10^{-3}, and 6.8×10^{-3} at 25, 35, 40, and 45 °C, respectively, with a reaction order always in the range 1.4–1.42. Therefore, the synthetic phenol solution photodegradation was characterized by faster kinetics in comparison with that observed for OMW phototreatment. Even if a proper comparison cannot be made, OMW is very complex wastewater, containing various recalcitrant pollutants in addition to phenol compounds. Guo and coworkers [49] reported an optimal pH equal to 6 for phenol's photodegradation, below the pH of zero-charge of the photocatalyst (TiO_2-SiO_2) used here and achieving a total removal above 85% in 140 min.

Finally, the apparent kinetic constant variation with T has been modeled using the Arrhenius model (Figure 6).

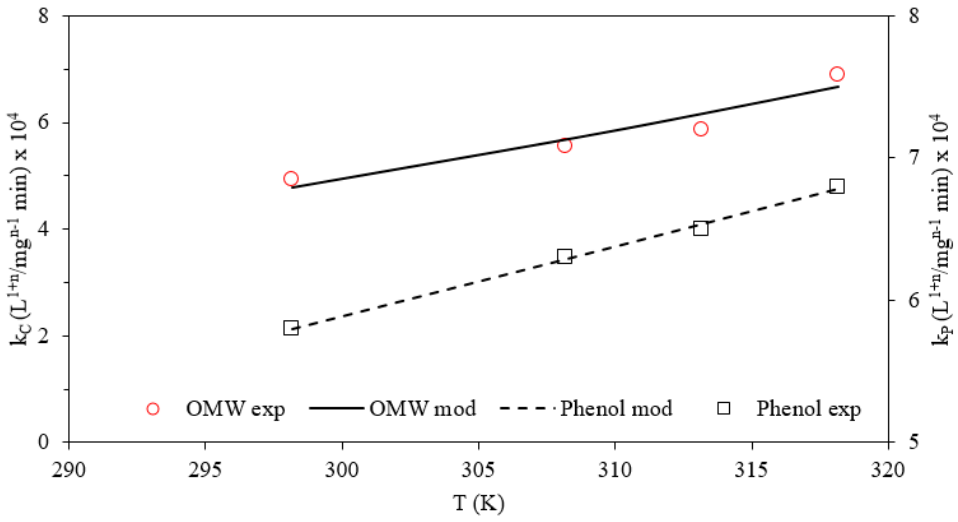

Figure 6. Kinetic constant values at different temperatures (point) and fitted Arrhenius model (line) (T = 25, 35, 40, and 45 °C; initial OMW COD = 9.4 g L^{-1}; synthetic solution initial concentration = 25 mg L^{-1}; impeller rotational velocity = 200 rpm).

The regressed parameters are reported in Table 1.

Table 1. Regressed parameters of photocatalysis kinetic modelling.

	OMW	Synthetic Phenol
k_0 (L^{1+n}/min mg^{n-1})	0.024	0.7
E (kJ mol^{-1})	9.57	6.17

The pre-exponential factor of phenol's kinetics was higher in comparison to that of OMW, as well as the apparent activation energy was lower. The E value for OMW cannot be properly considered an activation energy, since this wastewater is a complex of several organic and inorganic compounds, whereas E can be defined only for a single compound; therefore, the results obtained cannot be directly compared, but can be useful to better characterize the photodegradation kinetics of this particular two-phase OMW.

4. Conclusions

In this study, a sequential batch process was proposed and applied to treat real olive mill wastewater streams. The first step was a coagulation/flocculation process, using chitosan at 500 mg L^{-1} as a coagulant. The results obtained showed a reduction of turbidity and chemical oxygen demand of 90% and 33%, respectively. The kinetic of the process was interpreted according to Smoluchowski's theory (perikinetic model) and a kinetic constant of 6.68×10^{-4} L^{1+n}/min mg^{n-1} was estimated. Subsequently, laboratory-made nanophotocatalyst particles were employed using pretreated wastewater and a synthetic phenol solution. The photocatalysis kinetic process was analyzed at different temperature values. In detail, employing the optimal catalyst concentration for the two solutions, that is 1.5 and 2 g L^{-1}, for synthetic phenol and olive mill wastewater, respectively, a phenol removal of 90% and a COD removal efficiency of 45.8% were reached. The Arrhenius model fit the data well for describing the kinetic constant-temperature trends for both reactions.

Author Contributions: Conceptualization, S.V. and M.S.; methodology, S.V.; investigation, S.V.; resources, S.V. and M.S.; data curation, S.V.; writing—original draft preparation, S.V.; writing—review and editing, M.S.; supervision, M.S. All authors have read and agreed to the published version of the manuscript.

Funding: This research received no external funding.

Acknowledgments: Author (Srikanth Vuppala) acknowledges the XXXI Cycle-International PhD fellowships, La Sapienza University of Rome, for providing full fellowship to pursue the PhD and finish the research work.

Conflicts of Interest: The authors declare no conflict of interest. The funders had no role in the design of the study; in the collection, analyses, or interpretation of data; in the writing of the manuscript, or in the decision to publish the results.

References

1. Bora, T.; Dutta, J. Applications of nanotechnology in wastewater treatment—A review. *J. Nanosci. Nanotechnol.* **2014**, *14*, 613–626. [CrossRef] [PubMed]
2. Vilardi, G. Mathematical modelling of simultaneous nitrate and dissolved oxygen reduction by Cu-nZVI using a bi-component shrinking core model. *Powder Technol.* **2019**, *343*, 613–618. [CrossRef]
3. Abdelbasir, S.M.; Shalan, A.E. An overview of nanomaterials for industrial wastewater treatment. *Korean J. Chem. Eng.* **2019**, *36*, 1209–1225. [CrossRef]
4. Davies, L.C.; Vilhena, A.; Novais, J.M.; Martins-Dias, S. Modelling of olive mill wastewater characteristics. *WIT Trans. Ecol. Environ.* **2003**, *65*, 313–322, ISSN 1743-3541.
5. Vavouraki, A.I.; Zakoura, M.V.; Dareioti, M.A.; Kornaros, M. Biodegradation of Polyphenolic Compounds from Olive Mill Wastewaters (OMW) during Two-stage anaerobic Co-digestion of Agro-industrial mixtures. *Waste Biomass Valorization* **2019**. [CrossRef]
6. Sáez, J.A.; Pérez-Murcia, M.D.; Martínez-Gallardo, M.R.; Andreu-Rodríguez, F.J.; López, M.J.; Bustamante, M.A.; Sanchez-Hernandez, J.C. Olive mill wastewater-evaporation ponds long term stored: Integrated assessment of in situ bioremediation strategies based on composting and vermicomposting. *J. Hazard. Mater.* **2020**, *402*, 123481. [CrossRef]
7. Enaime, G.; Baçaoui, A.; Yaacoubi, A.; Berzio, S.; Wichern, M.; Lübken, M. Packed-bed biofilm reactor for semi-continuous anaerobic digestion of olive mill wastewater: Performances and COD mass balance analysis. *Environ. Technol.* **2020**, *41*, 2657–2669. [CrossRef] [PubMed]
8. Ochando-Pulido, J.M.; Vellido-Pérez, J.A.; González-Hernández, R.; Martínez-Férez, A. Optimization and modeling of two-phase olive-oil washing wastewater integral treatment and phenolic compounds recovery by novel weak-base ion exchange resins. *Sep. Purif. Technol.* **2020**, *249*, 117084. [CrossRef]
9. Gernjak, W.; Maldonado, M.I.; Malato, S.; Cáceres, J.; Krutzler, T.; Glaser, A.; Bauer, R. Pilot-plant treatment of olive mill wastewater (OMW) by solar TiO_2 photocatalysis and solar photo-Fenton. *Sol. Energy* **2004**, *77*, 567–572. [CrossRef]
10. Voros, V.; Drioli, E.; Fonte, C.; Szekely, G. Process intensification via continuous and simultaneous isolation of antioxidants: An upcycling approach for olive leaf waste. *ACS Sustain. Chem. Eng.* **2019**, *7*, 18444–18452. [CrossRef]

11. Didaskalou, C.; Buyuktiryaki, S.; Kecili, R.; Fonte, C.P.; Szekely, G. Valorisation of agricultural waste with an adsorption/nanofiltration hybrid process: From materials to sustainable process design. *Green Chem.* **2017**, *19*, 3116–3125. [CrossRef]
12. Paradiso, V.M.; Clemente, A.; Summo, C.; Pasqualone, A.; Caponio, F. Towards green analysis of virgin olive oil phenolic compounds: Extraction by a natural deep eutectic solvent and direct spectrophotometric detection. *Food Chem.* **2016**, *212*, 43–47. [CrossRef]
13. Jerman Klen, T.; Vodopivec, B.M. Optimisation of olive oil phenol extraction conditions using a high-power probe ultrasonication. *Food Chem.* **2012**, *134*, 2481–2488. [CrossRef] [PubMed]
14. Otles, S. Treatment of olive mill wastewater and the use of polyphenols obtained after treatment. *Int. J. Food Stud.* **2012**, *1*, 85–100. [CrossRef]
15. Stoller, M.; Di Palma, L.; Vuppala, S.; Vilardi, N.V. Process intensification techniques for the production of nano- and submicronic particles for food and medical applications. *Curr. Pharm. Des.* **2018**, *24*, 2329–2338. [CrossRef] [PubMed]
16. Choquette-Labbé, M.; Shewa, W.; Lalman, J.; Shanmugam, S. Photocatalytic degradation of phenol and phenol derivatives using a Nano-TiO_2 catalyst: Integrating quantitative and qualitative factors using response surface methodology. *Water* **2014**, *6*, 1785–1806. [CrossRef]
17. Wong, C.L.; Tan, Y.N.; Mohamed, A.R. Photocatalytic degradation of phenol using immobilized TiO_2 nanotube photocatalysts. *J. Nanotechnol.* **2011**, *2011*, 1–9. [CrossRef]
18. Zhang, L.; Jia, Z.; Lyu, F.; Liang, S.; Lu, J. Progress in materials science a review of catalytic performance of metallic glasses in wastewater treatment: Recent progress and prospects. *Prog. Mater. Sci.* **2019**, *105*, 100576. [CrossRef]
19. Liang, S.X.; Jia, Z.; Liu, Y.J.; Zhang, W.; Wang, W.; Lu, J.; Zhang, L.C. Compelling rejuvenated catalytic performance in metallic glasses. *Adv. Mater.* **2018**, *30*, e1802764. [CrossRef]
20. Liang, S.; Wang, X.; Zhang, W.; Liu, Y.; Wang, W.; Zhang, L. Selective laser melting manufactured porous Fe-based metallic glass matrix composite with remarkable catalytic activity and reusability. *Appl. Mater. Today* **2020**, *19*, 100543. [CrossRef]
21. Ruíz-Delgado, A.; Roccamante, M.A.; Malato, S.; Agüera, A.; Oller, I. Olive mill wastewater reuse to enable solar photo-Fenton-like processes for the elimination of priority substances in municipal wastewater treatment plant effluents. *Environ. Sci. Pollut. Res. Int.* **2020**, *27*, 38148–38154. [CrossRef]
22. Chianese, S.; Fenti, A.; Iovino, P.; Musmarra, D.; Salvestrini, S. Sorption of organic pollutants by humic acids: A review. *Molecules* **2020**, *25*, 918. [CrossRef]
23. Vilardi, G.; Di Palma, L.; Verdone, N. Chinese journal of chemical engineering heavy metals adsorption by banana peels micro-powder: Equilibrium modeling by non-linear models. *Chin. J. Chem. Eng.* **2018**, *26*, 455–464. [CrossRef]
24. Rizzo, L.; Lofrano, G.; Grassi, M.; Belgiorno, V. Pre-treatment of olive mill wastewater by chitosan coagulation and advanced oxidation processes. *Sep. Purif. Technol.* **2008**, *63*, 648–653. [CrossRef]
25. Hamdi, M.; Garcia, J.L.; Ellouz, R. Integrated biological process for olive mill wastewater treatment. *Bioprocess Eng.* **1992**, *8*, 79–84. [CrossRef]
26. Vilardi, G.; Rodriguez-Rodriguez, J.; Ochando-Pulido, J.M.; Di Palma, L.; Verdone, N. Fixed-bed reactor scale-up and modelling for Cr(VI) removal using nano iron-based coated biomass as packing material. *Chem. Eng. J.* **2019**, *361*, 990–998. [CrossRef]
27. Borges, M.E.; Sierra, M.; Cuevas, E.; García, R.D.; Esparza, P. Photocatalysis with solar energy: Sunlight-responsive photocatalyst based on TiO_2 loaded on a natural material for wastewater treatment. *Sol. Energy* **2016**, *135*, 527–535. [CrossRef]
28. You, J.; Guo, Y.; Guo, R.; Liu, X. A review of visible light-active photocatalysts for water disinfection: Features and prospects. *Chem. Eng. J.* **2019**, *373*, 624–641. [CrossRef]
29. Hennig, H.; Billing, R. Advantages and disadvantages of photocatalysis induced by light-sensitive coordination compounds. *Coord. Chem. Rev.* **1993**, *125*, 89–100. [CrossRef]
30. Fedotova, M.P.; Voronova, G.A.; Emelyanova, E.Y.; Vodyankina, O.V. A method of preparation of active TiO_2-SiO_2 photocatalysts for water purification. *Stud. Surf. Sci. Catal.* **2010**, *175*, 723–726. [CrossRef]
31. Nguyen, V.-C.; Nguyen, T.-V. Photocatalytic decomposition of phenol over N–TiO_2–SiO_2 catalyst under natural sunlight. *J. Exp. Nanosci.* **2009**, *4*, 233–242. [CrossRef]

32. Stoller, M.; Vuppala, S.; Matarangolo, M.; Vaiano, V.; Sannino, D.; Chianese, A.; Cianfrini, C. About a novel production method for N-doped magnetic nanocore nanoparticles of titania by means of a spinning disk reactor. *Chem. Eng. Trans.* **2017**, *60*, 43–48. [CrossRef]
33. Liang, S.; Zhang, W.; Zhang, L.; Wang, W.; Zhang, L. Remediation of industrial contaminated water with arsenic and nitrate by mass-produced Fe-based metallic glass: Toward potential industrial applications. *Sustain. Mater. Technol.* **2019**, *22*, e00126. [CrossRef]
34. De Caprariis, B.; Di Rita, M.; Stoller, M.; Verdone, N.; Chianese, A. Reaction-precipitation by a spinning disc reactor: Influence of hydrodynamics on nanoparticles production. *Chem. Eng. Sci.* **2012**, *76*, 73–80. [CrossRef]
35. Sacco, O.; Vaiano, V.; Rizzo, L.; Sannino, D. Photocatalytic activity of a visible light active structured photocatalyst developed for municipal wastewater treatment. *J. Clean. Prod.* **2018**, *175*, 38–49. [CrossRef]
36. Vaiano, V.; Sacco, O.; Sannino, D.; Ciambelli, P.; Longo, S.; Venditto, V.; Guerra, G. N-doped TiO_2/s-PS aerogels for photocatalytic degradation of organic dyes in wastewater under visible light irradiation. *J. Chem. Technol. Biotechnol.* **2014**, *89*, 1175–1181. [CrossRef]
37. Nieto, L.M.; Hodaifa, G.; Rodríguez, S.; Giménez, J.A.; Ochando, J. Flocculation-sedimentation combined with chemical oxidation process. *Clean Soil Air Water* **2011**, *39*, 949–955. [CrossRef]
38. Association, A.P.H.; Eaton, A.D.; Association, A.W.W.; Federation, W.E. *Standard Methods for the Examination of Water and Wastewater*; APHA-AWWA-WEF: Washington, DC, USA, 2005; ISBN 0875530478 9780875530475.
39. Reymond, J.P.; Kolenda, F. Estimation of the point of zero charge of simple and mixed oxides by mass titration. *Powder Technol.* **1999**, *103*, 30–36. [CrossRef]
40. Paul, T.; Miller, P.L.; Strathmann, T.J. Visible-light-mediated TiO_2 photocatalysis of fluoroquinolone antibacterial agents. *Environ. Sci. Technol.* **2007**, *41*, 4720–4727. [CrossRef]
41. Chatzisymeon, E.; Xekoukoulotakis, N.P.; Mantzavinos, D. Determination of key operating conditions for the photocatalytic treatment of olive mill wastewaters. *Catal. Today* **2009**, *144*, 143–148. [CrossRef]
42. Cheng, D.; Ariafar, S.; Sheibat-Othman, N.; Pohn, J.; McKenna, T.F.L. Particle coagulation of emulsion polymers: A review of experimental and modelling studies. *Polym. Rev.* **2018**, *58*, 1–43. [CrossRef]
43. Ani, J.U.; Nnaji, N.J.N.; Onukwuli, O.D.; Okoye, C.O.B. Nephelometric and functional parameters response of coagulation for the purification of industrial wastewater using Detarium microcarpum. *J. Hazard. Mater.* **2012**, *243*, 59–66. [CrossRef] [PubMed]
44. Vuppala, S.; Bavasso, I.; Stoller, M.; Di Palma, L.; Vilardi, G. Olive mill wastewater integrated purification through pre-treatments using coagulants and biological methods: Experimental, modelling and scale-up. *J. Clean. Prod.* **2019**, *236*, 117622. [CrossRef]
45. Rizzo, L.; Lofrano, G.; Belgiorno, V. Olive mill and winery wastewaters pre-treatment by coagulation with chitosan. *Sep. Sci. Technol.* **2010**, *45*, 2447–2452. [CrossRef]
46. Kumar, M.M.; Karthikeyan, R.; Anbalagan, K.; Bhanushali, M.N. Coagulation process for tannery industry effluent treatment using Moringa oleifera seeds protein: Kinetic study, pH effect on floc characteristics and design of a thickener unit. *Sep. Sci. Technol.* **2016**, *51*, 2028–2037. [CrossRef]
47. Okolo, B.; Menkiti, M.; Nnaji, P.; Onukwuli, O.; Agu, C. The Performance of Okra seed (*Hibiscus esculentus* L.) Extract in Removal of Suspended Particles from Brewery Effluent by Coag-Flocculation Process. *Br. J. Appl. Sci. Technol.* **2014**, *4*, 4791–4806. [CrossRef]
48. Ruzmanova, Y.; Ustundas, M.; Stoller, M.; Chianese, A. Photocatalytic Treatment of olive mill wastewater by N-doped titanium dioxide nanoparticles under visible light. *Chem. Eng. Trans.* **2013**, *32*, 2233–2238. [CrossRef]
49. Guo, N.; Liang, Y.; Lan, S.; Liu, L.; Ji, G.; Gan, S.; Zou, H.; Xu, X. Uniform TiO_2-SiO_2 hollow nanospheres: Synthesis, characterization and enhanced adsorption-photodegradation of azo dyes and phenol. *Appl. Surf. Sci.* **2014**, *305*, 562–574. [CrossRef]